Development and characterization of silica tube-coated separator for lithium ion batteries

CrossMark

Peng Zhang [a], Lixiao Chen [b], Chuan Shi [b], Pingting Yang [a], Jinbao Zhao [a, b, *]

[a] College of Energy, Xiamen University, Xiamen 361102, China
[b] College of Chemistry & Chemical Engineering, Collaborative Innovative Center of Chemistry for Energy Materials, State Key Lab for Physical Chemistry of Solid Surface, Xiamen University, Xiamen 361005, China

HIGHLIGHTS

- Ceramic coating separator was developed with one-dimensional silica tubes (ST).
- The ST coating separator exhibits better thermal stability.
- The inorganic mesh network prevents the thermal shrinkage of the separator.
- The coating method is introduction ceramics to one side of PE separator.

ARTICLE INFO

ABSTRACT

In an endeavor to improve the thermal stability of lithium-ion batteries (LIBs), a new kind of ceramic coated separator has been developed based on introducing one-dimensional silica tubes (ST) to one side of a commercial polyethylene (PE) porous separator. The ST interpenetrating network diminishes the thermal-induced dimensional change of the commercial separator without compromising the cell performance. In particular, compared to spherical silica particle (SP) coated separator, the ST coated separator exhibits significantly enhanced thermal stability at elevated temperature. Furthermore the ST coated separator shows better mechanical performance as well as the improved electrolyte absorption and retention behavior, which provides a promising solution to replace conventional polymer separator for high-performance LIBs.

1. Introduction

Lithium ion batteries (LIBs) are the most widely used power sources for portable electronic products such as laptop computers and cellular phones attributed to the high energy density and long lifespan [1–4]. They also provide a stepping stone for the practical implementation of renewable intermittent energy sources and substantial reduction of fossil fuel consumption for transportation [3,5,6]. However, the widespread application of large-size LIBs in electric vehicles and smart grids has been hindered by the safety issue of LIB techniques [7–10]. One of the major concerns related to

the safe operation of LIBs is the poor thermal stability and inferior electrolyte wettability of standard separator materials, e.g. microporous polyethylene (PE) or polypropylene (PP) membranes for current LIBs, resulting in intolerable unreliability for long-term operation and sustainable high-power delivery [11,12].

Current PE and PP membranes have relatively low melting points of ~135 °C and 165 °C, respectively. Above the melting point, the thermally induced shrinking of the film closes the pores, and stops lithium ion transportation, thus it serves as a fail-safe device in LIB. However, in spite of acceptable transition temperatures, mechanical strength and electrochemical inertness, the morphology change of PE and PP at elevated temperature leads to incomplete isolation of cathode and anode, which results in internal short-circuit and catastrophic cell failure [12–14]. To address this issue, much efforts have been devoted to minimize the shrinkage of separator upon thermal shock [15,16], amongst which

* Corresponding author. College of Chemistry & Chemical Engineering, Collaborative Innovative Center of Chemistry for Energy Materials, State Key Lab for Physical Chemistry of Solid Surface, Xiamen University, Xiamen 361005, China.
E-mail address: jbzhao@xmu.edu.cn (J. Zhao).

introducing ceramic coating layer on single or both sides of polyolefin membranes has been demonstrated as an efficient approach [17–19], since: (1) the incorporation of inorganic ceramic powders results in high thermal resistance [20–22]; (2) the ceramic layer improves the compatibility of polymer separator toward polar electrolyte effectively, and consequentially improves electrolyte uptake and retention by the separator [20].

Recent studies confirm that inorganic particles with various morphologies may influence the performance of separator differently [23–25]. For example, Sang et al. reported that the effects of ceramic coating layers on the separator properties were in great detail investigated as a function of SiO_2 powder size, which demonstrated that the structure control of SiO_2 ceramic coating layers plays a crucial role in determining the composite separator properties [26]. One-dimensional nanostructured inorganic materials, such as nanowires are speculated to be better candidates for high-performance separators, since the interconnected 1D nanowires lead to the formation of robust networks resistant to mechanical deformation [27]. It has been reported that composite polymer electrolytes with SiO_2 nanowires displayed improved electrochemical and mechanical characteristics than that with SiO_2 nanoparticles [28]. There is only short range interaction among nanoparticles for Zero-dimensional spheres, while 1D nanowires exist long range interaction. The long range interaction may be beneficial for the prevention of the deformation. However, according to our knowledge, there is no report on the use of one-dimensional inorganic materials as coating material to obtain ceramic coated separators. In this paper, we report for the first time the preparation and the evaluation of physical and electrochemical properties of a new ceramic separator with silica tubes (ST) coating layer on porous PE separator. For a comparison, a ceramic coated separator with the same diameter of silica spheres is also prepared.

2. Experimental

2.1. The preparation of ST coated separator and SP coated separator

Silica sphere (SP) was synthesized by a precipitation method [29]. Ethyl acetate (13 g) was added to a mixed aqueous solution (131 g) of cetyltrimethylammonium bromide (CTAB, 7.5 g) and sodium silicate (8.4 g) under vigorous stirring. The precipitates were isolated by filtration and washed thoroughly with deionized water and ethanol several times.

Silica tube was synthesized using a reverse-microemulsion-mediated sol–gel method [30]. 9 g sodium bis(2-ethylhexyl) sulfosuccinate was dissolved in 40 mL hexane, and 0.4 mL 17 M $FeCl_3$ aqueous solution was introduced to the mixture, followed by addition of 1 g tetraethyl orthosilicate (TEOS). After standing for 10 h, 0.72 mL 4 M sodium hydroxide aqueous solution was introduced, and the powders were isolated by filtration and washed with ethanol to remove the surfactants and reagents.

The prepared silica tubes and spheres were pre-mixed with styrene butadiene rubber (SBR) (Guangzhou Songbai Chemical, China) and carboxyl methyl cellulose (CMC) (Guangzhou Songbai Chemical, China) respectively, at a weight ratio of 95:2:3 in a water/ethanol (1:1, v/v) mixture. The suspensions were then vigorously stirred for 3 h with a magnetic stirrer. A PE separator (thickness = 20 μm, Asahi Kasei, Japan) was selected as the coating substrate. The ST and SP slurries were coated onto one side of the PE membrane using an automatic coating machine (Shanghai environmental engineering technology Co., Ltd, China). The ceramic coated membranes were dried at room temperature and then further dehydrated under vacuum at 60 °C for 12 h.

2.2. Characterization of the separators

The morphologies of as-prepared ST and SP as well as ST and SP coated separators were investigated using a field emission scanning electron microscope (FE-SEM, S-4800, Hitachi, Japan). The thickness of coated separators was measured using a digital caliper. To examine the thermal stability, the separators were subjected to heat treatment at various temperatures for 0.5 h, and the final dimensions and area were measured using a ruler. The thermal shrinkage was calculated using the following equation:

$$\text{Thermal shrinkage}(\%) = (S_1 - S_2)/S_1 \times 100$$

where S_1 and S_2 refer to the area of separators before and after heat treatment. Mechanical measurement was carried out with an electronic universal testing machine (Shenzhen Suns Technology Stock Co. Ltd., China).

To demonstrate the safety performance of cells assembled with the PE separator, SP and ST coated separators at high temperature, pouch cells were assembled by sandwiching the separators between $LiCoO_2$ cathode and graphite anode. The cells were charged to 4.35 V at room temperature and then placed in a vacuum oven for a measurement of the open circuit voltage (OCV) at 130 °C using an electrochemical working station (AutoLab Sino-Metrohm Technology Ltd.) by monitoring the OCV of the cells as a function of time.

The wettability of the separator was studied by placing a drop of liquid electrolyte on the separator and measuring the contact angle using a Powereach JC2000C1 drop shape analysis system (Shanghai Zhong Chen Digital Technique Equipment Co. Ltd., China). The electrolyte uptake of separators was examined by measuring the weight increase of separators before and after immersed in the electrolyte for 1 min. The electrolyte uptake was calculated according to the following equation:

$$\text{Electrolyte uptake}(\%) = (W - W_0)/W_0$$

where W_0 and W are the mass of separators before and after immersion.

The ionic conductivity of the silica coated separators was measured in blocking-type cells fabricated by sandwiching them between two stainless steel electrodes. Impedance data were obtained with a Solartron SI 1260 impedance analyzer at a frequency range of 1 Hz–100 kHz. The ionic conductivity σ was calculated using equation:

$$\sigma = d/(R_b*S)$$

where d is the thickness of the separator, S is the area of the separator and R_b is the real impedance.

Lithium half-cells (2016-type coin) were assembled by sandwiching the separator between a lithium foil and a $LiMn_2O_4$ electrode. The composition of $LiMn_2O_4$ electrode was active material (Qingdao Shuangxing Co., China): Super P: PVDF = 90:5:5 w/w. The electrolyte consisted of 1 M $LiPF_6$ in EC, DEC and DMC (1:1:1, v/v) mixture. The cells were assembled in a Mbraun glove box filled with argon, and galvanostatic cycling was carried out using a LAND-V34 battery test equipment at a constant charge/discharge current density of 0.5C in the voltage range of 3.0–4.3 V and at a constant voltage of 4.3 V with the cut-off current density of 0.05C. Rate capabilities were measured at various charge/discharge current densities from 0.2C to 2C in the voltage range of 3.0–4.3 V.

3. Results and discussion

SiO_2 tube (ST) and SiO_2 microspheres (SP) were synthesized.
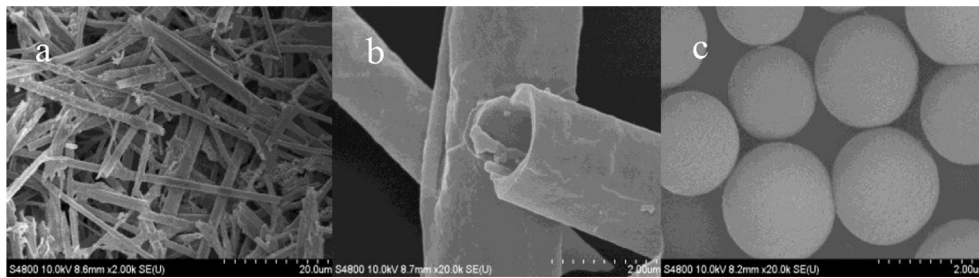
Fig. 1. SEM images of (a) silica tubes, (b) cross-section of silica tubes, and (c) silica spheres.

Fig. 1a and b shows the SEM images of the as-prepared ST. The ST is straight and smooth, with lengths of 20–40 μm and a narrow diameter distribution. The thickness and outer diameter of the tube wall are approximately 20–30 nm and 1–2 μm, respectively. The SP as shown in Fig. 1c exhibit a monodisperse size distribution and have a uniform spherical shape with an average diameter around 1–2 μm, which is similar to the outer diameter of ST. Therefore, it is more rational to compare the thermal and electrochemical performance of the ceramic coated separators prepared with ST and SP.

Fig. 2 shows the top view and cross section of the separators coated with ST and SP, respectively. The ST and SP are both successfully conglutinated onto the surface of PE separators, leading to continuous and uniform coatings of ~9 μm thick (Fig. 2a and c). The ST and SP are homogeneously distributed in the surface layer without agglomeration. Highly connected interstitial voids form between the ceramic powder particles, affording a well-developed porous structure, which is expected to be filled with the liquid electrolyte and provide a facile pathway for ion movement in addition to improving the wettability of the separator. Furthermore, the 1-D network constructed from ST contains randomly

distributed and interconnected ST, potentially providing numerous interpenetrating channels for rapid electrolyte diffusion. In contrast, the SP coating is much more compact. The cross-sectional morphology shown in Fig. 2b and d reveals that ST and SP are deposited uniformly and that the coating layer is approximately 9 μm thick, which is relatively thin for coatings obtained using a laboratory technique.

As is well known, the thermostability of the separators plays a vital role in preventing internal short circuits between the electrodes when the batteries are exposed to high temperature, which is especially important for the large-scale LIBs being developed for electric vehicles and energy storage systems. However, the PE separator has a melting point of approximately 135 °C and easily loses dimensional stability upon exposure to high temperatures above 100 °C. The morphology variation of ST and SP coated PE separators along with pristine PE separator upon heating to >130 °C is illustrated in Fig. 3. All the separators were subjected to heat treatment at 150 °C for 30 min. The pristine PE separator turns from opaque to transparent and exhibits the largest thermal shrinkage of 70% (Fig. 3a). The ST coated separator is most robust
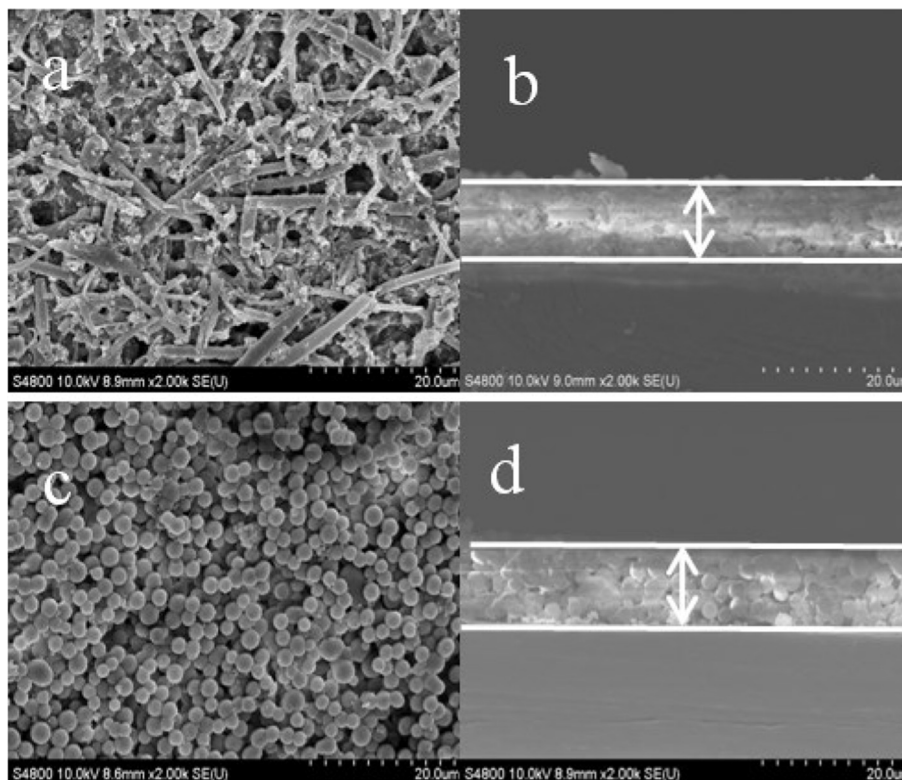

Fig. 2. SEM images of (a) surface and (b) cross-section of ST coating separator, (c) surface and (d) cross-section of SP coating separator.

Fig. 3. Dimensions of separators before and after subjected to heat treatment at 150 °C for 30 min (a) pristine PE separator; (b) ST coating separator; (c) SP coating separator.

toward thermal treatment, showing a thermal shrinkage of 18.95% (Fig. 3b), and the SP coated separator shrinks 54.1% (Fig. 3c). To achieve an incremental temperature increase as an analog of real LIBs, the temperature was also raised step by step, and the thermal shrinkage as a function of temperature of the above three systems are depicted in Fig. 4. The bare PE separator shrinks about 5% at 110 °C, while there is no visual change of the SP and ST coated separators. The ST coated separator, on the other hand, remains intact at 120 °C, while the SP coated separator shrinks 5%. This improvement in the thermal shrinkage of the SP and ST coated separator is ascribed to the existence of ceramic coating layers. The heat-resistant SiO_2 particles are believed to effectively prevent the composite separator from being thermally shrunk. Moreover, the ST coated separator has better thermal stability than the SP coated separator. The larger thermal resistance of ST coating could be explained by an improved robustness resulting from the inter-twined 1-D mesh-like structure and one-dimensional materials usually have good tensile strength, which is verified by the mea-surement of mechanical stiffness as shown in Fig. 5. The tensile strength of ST (~1.13 MPa) coated separator is superior than that of SP coated separator (~1.05 MPa) due to numerous contacting points within the 1-D network.

To further study the safety performance of cells assembled with the PE separator and SP, ST coated separators, the °CV of pouch cells at 130 °C was measured. As shown in Fig. 6, the °CV curve of the cell based on the PE separator drops sharply to 0 V after 15 min, which shows obviously an internal short circuit of the cell. In contrast, the cells assembled with the SP and ST coated separators operates well even after 40 min, as the SP and ST coated separators maintain its dimensional stability and prevent the cell from experiencing an internal short circuit. Combining the features of thermal stability,
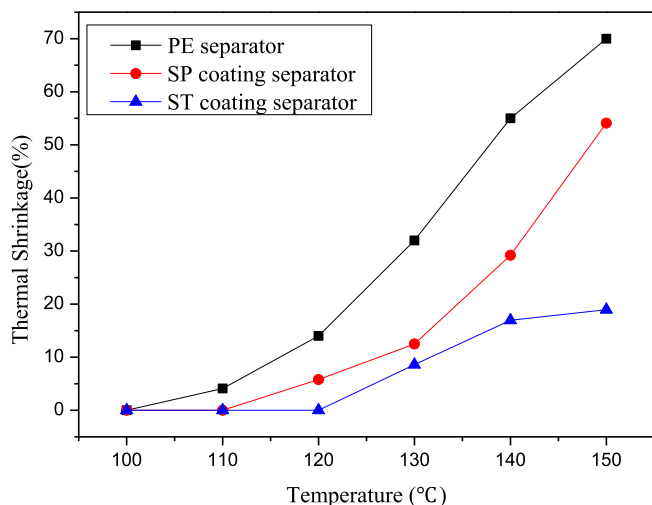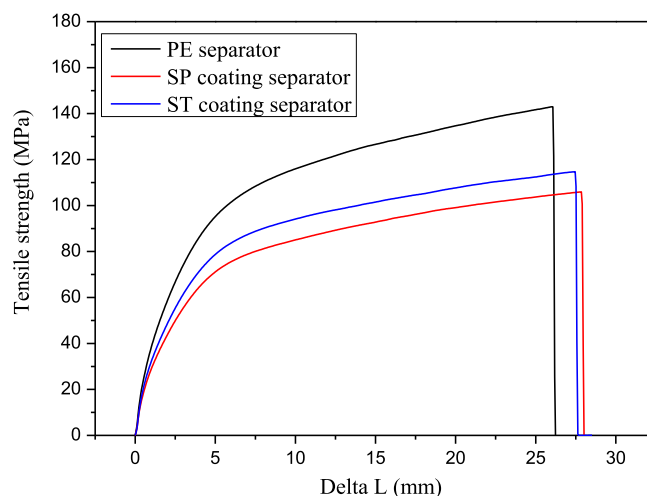

Fig. 5. Tensile strength at break for PE separator, SP coating separator and ST coating separator.

which protects the cells from internal short circuits, this SP and ST coated separators are expected to be attractive for battery systems requiring high safety.

Fig. 7 presents the results of electrolyte contact angle mea-surements on the three separators. The equilibrium contact angle of the electrolyte on the bare PE separator is 46.2° (Fig. 7a), while the electrolyte immediately spreads and fully penetrates into the sur-face of both SP and ST coated separators, leaving a contact angle of zero (Fig. 7b and c). Moreover, the electrolyte absorption behavior of the separators was investigated by immersing them in the
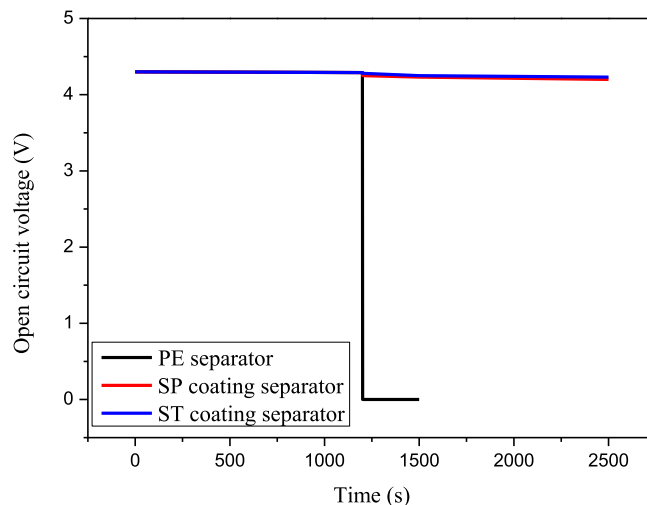

Fig. 4. Thermal shrinkage of pristine PE separator, ST coating separator and SP coating separator as a function of temperature.

Fig. 6. OCV curves of pouch cells assembled with PE separator, ST coating separator and SP coating separator.
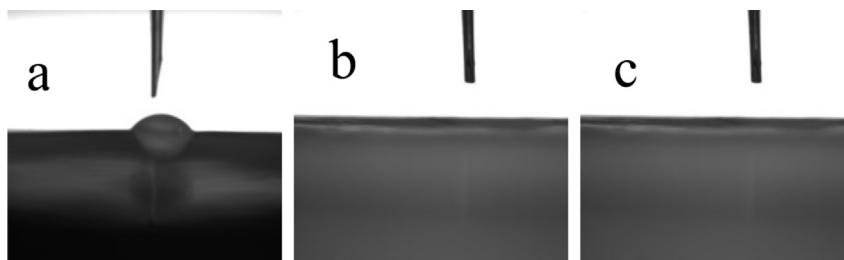
Fig. 7. Contact angle images of (a) pristine PE separator; (b) ST coating separator; (c) SP coating separator.

electrolyte. The mass of bare PE separator increases by 77% after immersing in the electrolyte, whereas the SP and ST coated separators show much higher electrolyte uptake of 105% and 112.5%. Both the ST and SP coating layers improve the wettability and electrolyte uptake, which may be ascribed to the high surface area and polarity of the inorganic SiO_2 structures and consequently a good affinity toward the polar electrolyte solvents [20,31]. The highest electrolyte uptake by the ST coated separator indicates that the tubular structure is most conducive to electrolyte reservation.

The enhanced electrolyte affinity of the coated separators was further evidenced by electrochemical impedance spectroscopy (EIS). Nyquist plots of all the separators show similar trends. The bare PE separator has the smallest equivalent circuit resistance because of the smallest total thickness. Calculated from the equivalent circuit model, the ionic conductivities of ST and SP coated separators are ~0.82 mS cm^{-1} and higher than that of the bare PE separator (0.62 mS cm^{-1}). The ionic conductivity of separator varies with several parameters, such as thickness, porosity, and tortuosity of the separator and kinetics of electrolyte infiltration [12]. Although the SiO_2 coating increases the total thickness of the separators, the higher ionic conductivity from the bilayer separators confirms the change of surface polarity of the separators by the SiO_2 coating, which further promotes the diffusion of Li ions across the separators.

Fig. 8 presents the cycling performance of cells assembled with the three separators. The cells were all charged/discharged up to 100 cycles at a constant current density of 0.5C in the voltage range of 3.0−4.3 V. The discharge specific capacity of the cells with ST coated separator is slightly lower comparing to that with the bare PE and SP coated separator. This is likely due to the lower coulombic efficiency of ST coated separators, which are about 95% for the first several cycles, as shown in Fig. 9. The possible explanation might be locally low porosity, which needs further research. However, the cell with ST coated separator does recover to a normal discharge specific capacity and after 100 cycles the discharge specific capacity is 102.5 mAh g^{-1}, which is comparable to 103 mAh g^{-1}of the pristine PE separator, as shown in Fig. 10. Fig. 11 shows the rate capabilities of cells assembled with PE separator, SP and ST coated separator. Compared to PE separator, the C-rate capacities of cells assemble with SP and ST coated separators appear to smaller increase, which reveal that the SP or ST coating does not significantly hinder ionic conduction. The previous results about ionic conductivities exhibit the similar situation. The ionic conductivities of the ST and SP coated separators are higher than the pristine PE separator. Overall, the ST ceramic coating layer does not compromise the cycling performance of batteries.

4. Conclusion

The silica tube coated separator has noticeably improved the thermal stability of the separator compared to common SP coated separator and the PE separator itself. The high structural resistance to thermal shrinkage of the ST coated separator may be due to the formation of 3-D mesh-like robust porous network by the one-dimensional ST. The ST coating on PE membrane alters its surface polarity from nonpolar to highly polarized, thus enhances electrolyte absorption and electrolyte retention. Based upon the cycling data of the cells in this study, the silica tubes coating does not compromise the cell performance.
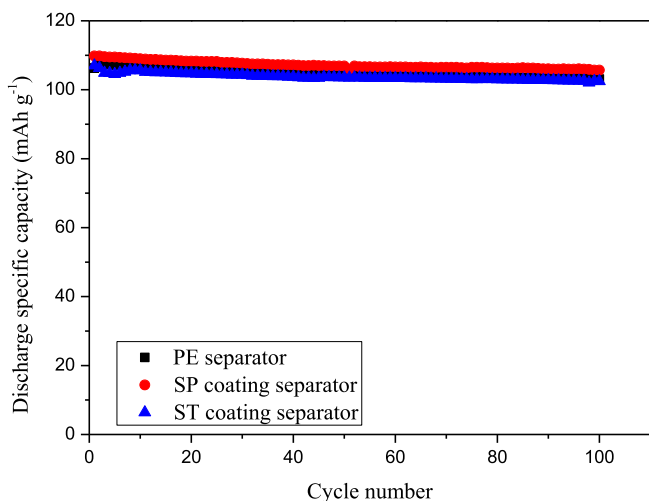

Fig. 8. Cycling performance of the cells assembled with PE separator, ST coating separator and SP coating separator.
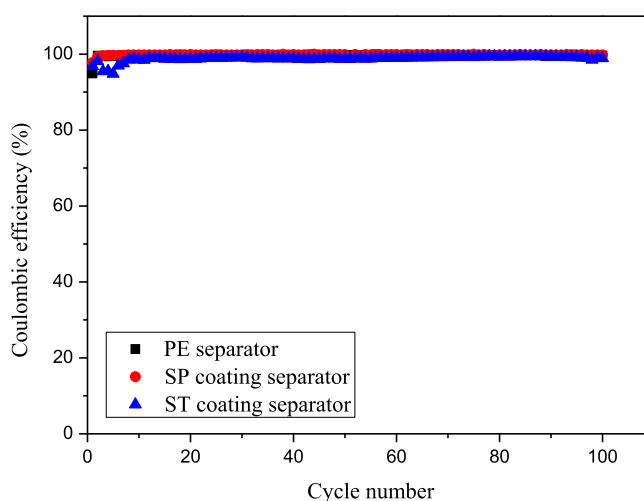

Fig. 9. Coulombic efficiency of the cells assembled with PE separator, ST coating separator and SP coating separator.
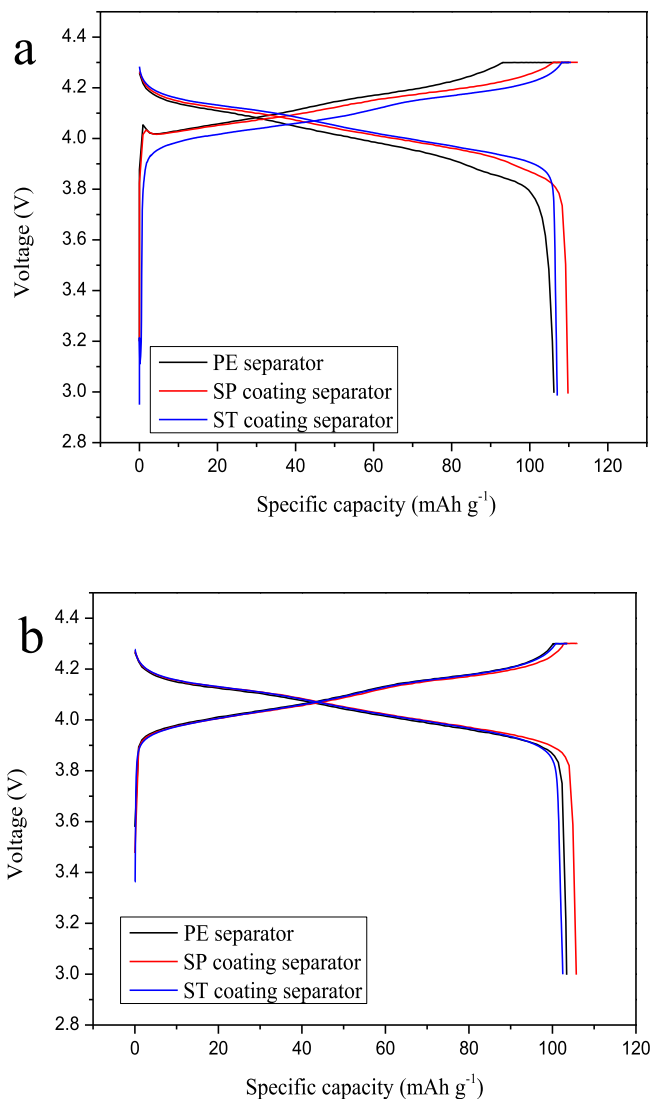
Fig. 10. Charge-discharge curves of the cells assembled with PE separator, ST coating separator and SP coating separator for (a) the 1st cycle and (b) the 100th cycle.
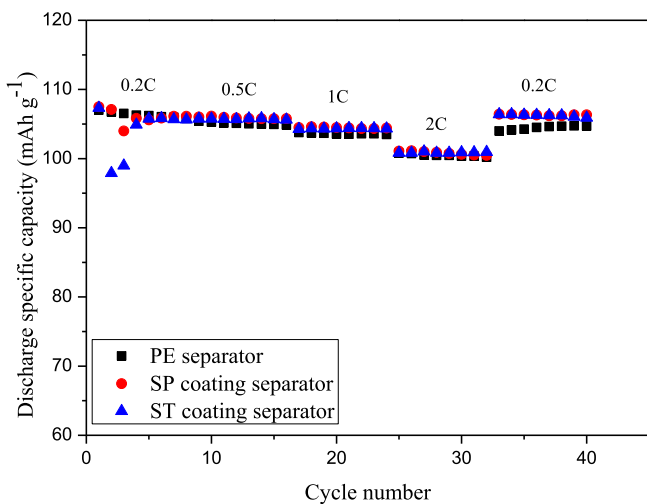

Fig. 11. Rate capabilities of cells assembled with PE separator, SP coating separator and ST coating separator at various current densities from 0.2C/0.2C to 2C/2C.

References

[1] T. Kawakatsu, T. Fukuoka, K. Tsutsui, I. Katsumata, Y. Hattori, Matsushita Tech. J. 52 (2006) 262−267.
[2] B.A. Johnson, R.E. White, J. Power Sources 70 (1998) 48−54.
[3] J.B. Goodenough, Y. Kim, Chem. Mater. 22 (2010) 587−603.
[4] W.-f An, B.-r Wu, K. Yang, H.-j Li, F. Wu, S. Chen, F. Chen, Dianchi Gongye 14 (2009) 318−321.
[5] J. Arai, T. Yamaki, S. Yamauchi, T. Yuasa, T. Maeshima, T. Sakai, M. Koseki, T. Horiba, J. Power Sources 146 (2005) 788−792.
[6] M.R. Palacin, Chem. Soc. Rev. 38 (2009) 2565−2575.
[7] K. Zaghib, P. Charest, A. Guerfi, J. Shim, M. Perrier, K. Striebel, J. Power Sources 134 (2004) 124−129.
[8] Y.-K. Sun, S.-T. Myung, B.-C. Park, J. Prakash, I. Belharouak, K. Amine, Nat. Mater. 8 (2009) 320−324.
[9] J. Graetz, F. Wang, in, Pan Stanford Publishing Pte. Ltd., 2014, pp. 69−94.
[10] K. Amine, J. Liu, S. Kang, I. Belharouak, Y. Hyung, D. Vissers, G. Henriksen, J. Power Sources 129 (2004) 14−19.
[11] G. Venugopal, J. Moore, J. Howard, S. Pendalwar, J. Power Sources 77 (1999) 34−41.
[12] P. Arora, Z. Zhang, Chem. Rev. Wash. D.C. U. S.) 104 (2004) 4419−4462.
[13] C.T. Love, J. Power Sources 196 (2011) 2905−2912.
[14] J. Song, M.-H. Ryou, B. Son, J.-N. Lee, D.J. Lee, Y.M. Lee, J.W. Choi, J.-K. Park, Electrochim. Acta 85 (2012) 524−530.
[15] D. Takemura, S. Aihara, K. Hamano, M. Kise, T. Nishimura, H. Urushibata, H. Yoshiyasu, J. Power Sources 146 (2005) 779−783.
[16] W. Jiang, Z. Liu, Q. Kong, J. Yao, C. Zhang, P. Han, G. Cui, Solid State Ionics 232 (2013) 44−48.
[17] J. Fang, A. Kelarakis, Y.-W. Lin, C.-Y. Kang, M.-H. Yang, C.-L. Cheng, Y. Wang, E.P. Giannelis, L.-D. Tsai, Phys. Chem. Chem. Phys. 13 (2011) 14457−14461.
[18] Y.S. Jung, A.S. Cavanagh, L. Gedvilas, N.E. Widjonarko, I.D. Scott, S.-H. Lee, G.-H. Kim, S.M. George, A.C. Dillon, Adv. Energy Mater. 2 (2012) 1022−1027.
[19] H.-S. Jeong, S.C. Hong, S.-Y. Lee, J. Membr. Sci. 364 (2010) 177−182.
[20] H.-S. Jeong, E.-S. Choi, S.-Y. Lee, J.H. Kim, J. Membr. Sci. 415−416 (2012) 513−519.
[21] M. Kim, J.H. Park, J. Power Sources 212 (2012) 22−27.
[22] C. Shi, P. Zhang, L. Chen, P. Yang, J. Zhao, J. Power Sources 270 (2014) 547−553.
[23] J.-H. Park, W. Park, J.H. Kim, D. Ryoo, H.S. Kim, Y.U. Jeong, D.-W. Kim, S.-Y. Lee, J. Power Sources 196 (2011) 7035−7038.
[24] J.-H. Park, J.-H. Cho, W. Park, D. Ryoo, S.-J. Yoon, J.H. Kim, Y.U. Jeong, S.-Y. Lee, J. Power Sources 195 (2010) 8306−8310.
[25] E.-S. Choi, S.-Y. Lee, J. Mater. Chem. 21 (2011) 14747−14754.
[26] H.-S. Jeong, S.-Y. Lee, J. Power Sources 196 (2011) 6716−6722.
[27] Y. Xia, P. Yang, Y. Sun, Y. Wu, B. Mayers, B. Gates, Y. Yin, F. Kim, H. Yan, Adv. Mater. Weinh. Ger.) 15 (2003) 353−389.
[28] P. Zhang, L.C. Yang, L.L. Li, M.L. Ding, Y.P. Wu, R. Holze, J. Membr, Sci. 379 (2011) 80−85.
[29] B. Wang, W. Shan, Y. Zhang, J. Xia, W. Yang, Z. Gao, Y. Tang, Adv. Mater. Weinh. Ger.) 17 (2005) 578−582.
[30] J. Jang, H. Yoon, Adv. Mater. Weinh. Ger.) 16 (2004) 799−802.
[31] J.-R. Lee, J.-H. Won, S.-Y. Lee, J. Electrochem. Sci. Technol. 2 (2011) 51−56.